

# LaF<sub>3</sub> core/shell nanoparticles for subcutaneous heating and thermal sensing in the second biological-window

Erving Clayton Ximendes,<sup>1,2</sup> Uéslen Rocha,<sup>2</sup> Kagola Upendra Kumar,<sup>1</sup> Carlos Jacinto,<sup>1</sup> and Daniel Jaque<sup>2,a)</sup>

<sup>1</sup>Grupo de Fotônica e Fluidos Complexos, Instituto de Física, Universidade Federal de Alagoas, 57072-970 Maceió, Alagoas, Brazil

<sup>2</sup>Fluorescence Imaging Group, Departamento de Física de Materiales C-04, Facultad de Ciencias, Instituto Nicolás Cabrera, Universidad Autónoma de Madrid, 28049 Madrid, Spain

(Received 16 March 2016; accepted 4 June 2016; published online 20 June 2016)

We report on Ytterbium and Neodymium codoped LaF<sub>3</sub> core/shell nanoparticles capable of simultaneous heating and thermal sensing under single beam infrared laser excitation. Efficient light-to-heat conversion is produced at the Neodymium highly doped shell due to non-radiative de-excitations. Thermal sensing is provided by the temperature dependent Nd<sup>3+</sup> → Yb<sup>3+</sup> energy transfer processes taking place at the core/shell interface. The potential application of these core/shell multifunctional nanoparticles for controlled photothermal subcutaneous treatments is also demonstrated. *Published by AIP Publishing.* [<http://dx.doi.org/10.1063/1.4954170>]

Photothermal therapy (PTT) is a therapeutic strategy in which photon energy is converted into heat to cause irreversible damage at the cellular level and that could efficiently treat a great variety of diseases including cancer tumors.<sup>1–3</sup> In particular, nanoparticle (NP) based PTTs are attracting great attention nowadays. They are based on the use of nanoheaters (NHs), which are NPs with large light-to-heat conversion efficiencies.<sup>4–6</sup> The selective incorporation of NHs into cancer cells or tumors provides the means by which a subsequent optical excitation produces a temperature increment that will only affect the tissues aimed to be treated. The net effects caused on cancer tumors during PTTs strongly depend on both the magnitude of the heating as well as the treatment duration.<sup>7–10</sup> In this regard, in order to achieve an efficient treatment and keep the collateral damage at minimum it is extremely necessary to have a temperature reading during NP based PTTs. As a consequence, there has been an increasing interest in the design of multifunctional luminescent NPs capable of simultaneous heating and thermal sensing under single power excitation as they would constitute significant building blocks toward the achievement of real controlled PTTs as well as subcutaneous studies.<sup>11</sup> Despite the continuously growing list of systems that could operate as simultaneous NHs and nanothermometers (NTHs), including polymeric NPs, quantum dots, nanodiamonds, metallic NPs, and rare earth-doped NPs, only a few of them show real potential of working subcutaneously.<sup>12–14</sup> This is so because most of them operate in the visible spectrum domain, where optical penetration into tissues is minimal. To avoid this limitation, it is necessary to shift their operation spectral range from the visible to the spectral infrared ranges where tissues become partially transparent (due to simultaneous attenuation in both tissue absorption and scattering), lying in the so-called *biological windows* (BW).<sup>15,16</sup> Traditionally, three biological windows are defined: the first extending

from 650 up to 950 nm, the second covering the infrared region about 1000–1350 nm and the third extending from 1500 up to 1750 nm.<sup>17</sup> In particular, the applicability in the second biological window (II-BW) opens up the possibility of not only deep tissue imaging but also of high contrast, autofluorescence free *in vivo* fluorescence thermal sensing, as it has already been demonstrated in imaging applications.<sup>18–25</sup> As an additional requirement, the multifunctional NPs to be used should operate under infrared radiation single beam excitation at wavelength avoiding any non-selective cellular damage. Recent studies dealing with the heating effects and the light-induced cytotoxicity during *in vitro* imaging experiments have pointed out 808 nm as an optimal excitation wavelength, since it simultaneously minimizes both the laser-induced thermal loading of the tissue and the intracellular photochemical damage.<sup>23,26–28</sup> The existence of high power, cost-effective laser diodes operating at 808 nm also makes this specific wavelength interesting from a technical point of view.

In this sense, the design and synthesis of a single NP capable of simultaneous heating and thermal sensing, and operating in the II-BW, appears to be especially captivating and, also, quite challenging. A potential way to join different structures or sub-structures in a single one is the use of the so called core/shell engineering.<sup>29,30</sup> Over the last years, the core/shell engineering has been used to achieve larger brightness, since the presence of the shell minimizes non-radiative interactions between core and surroundings. However, if both the core and shell units are optically active, the core/shell engineering can also be used to synthesize multifunctional nanostructures with pre-tailored properties, such as efficient two photon emission under non-heating laser excitation.<sup>31</sup>

In this work, we have designed and synthesized core/shell NPs that operate in the II-BW and that are capable of subcutaneous heating and thermal sensing under single beam 808 nm excitation. This work is based on two recent demonstrations: (i) the heating capacity of heavily Neodymium

<sup>a)</sup>Author to whom correspondence should be addressed. Electronic mail: [daniel.jaque@uam.es](mailto:daniel.jaque@uam.es)

doped  $\text{LaF}_3$  NPs and (ii) the infrared luminescence thermal sensing of Neodymium and Ytterbium co-doped core-shell  $\text{LaF}_3$  NPs.<sup>11,32</sup> The multifunctional agent here developed aim to join both functionalities in a single nanostructure. The NPs presented herein are based on a core/shell structure with an  $\text{Yb}^{3+}$  doped core (concentration of 10 mol. %) and a highly  $\text{Nd}^{3+}$  doped shell (concentration of 25 mol. %). Both ions were spatially separated due to selective doping during the synthesis procedure. A schematic representation of the NPs used all along this work (hereafter  $\text{Yb@Nd LaF}_3$  NPs) is depicted in Figure 1(a). A detailed description of the synthesis procedure can be found elsewhere.<sup>11</sup> By analyzing transmission electron microscopy (TEM) experiments carried out in both single-core and core/shell  $\text{LaF}_3$  NPs (not shown for the sake of brevity) we have estimated a core diameter of 15 nm and a shell thickness of 4.5 nm. TEM images also reveal similar size distributions and shapes to those reported by our group in previous works also dealing with  $\text{LaF}_3$  NPs fabricated by the same procedure.<sup>11</sup> Nevertheless, this does not affect the working principle demonstrated here. Additionally, the core/shell nature of the  $\text{LaF}_3$  NPs synthesized by the adopted procedure has been previously demonstrated by both energy-dispersive X-ray (EDX) and electron paramagnetic resonance (EPR) techniques.<sup>11,33</sup>

Under the proposed scheme (see Figure 1(b)), the shell would act as a donor unit absorbing the 808 nm radiation through the  $^4\text{I}_{9/2} \rightarrow ^4\text{F}_{5/2}$   $\text{Nd}^{3+}$  absorption. Then, a rapid phonon-assisted relaxation to the metastable  $^4\text{F}_{3/2}$  state takes place. Once at the metastable state, radiative de-excitation is possible to occur (solid lines in Figure 1(b)). In particular, for high concentration of  $\text{Nd}^{3+}$  ions in the shell (as it is our case), the non-radiative de-excitations become dominant over radiative ones and, consequently, the shell becomes a heating unit surrounding the core (indicated by the red contour in Figure 1(a)). Additionally, phonon-assisted cross relaxation and energy migration to killer impurities might play an important role in the heating process. A meticulous explanation can be found elsewhere.<sup>3</sup> Simultaneously, energy transfer processes at the core/shell interface lead to a relaxation of  $\text{Nd}^{3+}$  ions down to their ground state and to a simultaneous excitation of  $\text{Yb}^{3+}$  ions from the ground state to the  $^2\text{F}_{5/2}$  excited state, from which infrared emission is produced (see dashed curved arrow in Figure 1(b)). As a

consequence of this  $\text{Nd}^{3+} \rightarrow \text{Yb}^{3+}$  energy transfer, the core/shell NP shows an emission spectrum constituted by both the  $\text{Nd}^{3+}$  emission bands (centered at 900, 1060, and 1350 nm) and the  $\text{Yb}^{3+}$  one (centered at 1000 nm). Figure 1(c) shows the fluorescence images—at 1000, 1060, and 1350 nm—of a cuvette with water solution containing the  $\text{Yb@Nd LaF}_3$  NPs and reveals the simultaneous generation of both  $\text{Nd}^{3+}$  and  $\text{Yb}^{3+}$  emission bands. The homogeneous signal obtained from the whole cuvette displays the homogeneity of the colloidal solution. Figure 1(c) demonstrates that the luminescence generated by the  $\text{Yb@Nd LaF}_3$  NPs can easily be detected in an infrared imaging set-up, revealing therefore, their potential for *in vivo* application.

The relative contribution of  $\text{Nd}^{3+}$  and  $\text{Yb}^{3+}$  emissions to the overall emission of the core/shell NPs depends on the  $\text{Nd}^{3+} \rightarrow \text{Yb}^{3+}$  energy transfer efficiency as well as on the back transfer, which are both expected to be temperature dependent.<sup>34,35</sup> Therefore, this provides thermal sensitivity to our NPs. In order to evaluate such thermal sensing capability, the temperature dependence of the emission spectra generated by our core/shell NPs, under 808 nm excitation, was investigated in the 15–50 °C range (see Figure 2(a)). The fluorescence at each temperature was collected by using an optical system coupled to a high resolution spectrometer. All those measurements were performed under low excitation power density ( $0.2 \text{ W cm}^{-2}$ ) in order to keep self-heating effects at minimum. As it can be seen, the contribution of  $\text{Yb}^{3+}$  ions to the overall emission spectra decreases with increasing temperature—a result that well agrees with recent studies.<sup>11</sup> This opens up the possibility of using the ratio between the emitted intensity of  $\text{Nd}^{3+}$  ions at 1350 nm ( $^4\text{F}_{3/2} \rightarrow ^4\text{I}_{13/2}$ ) and that of  $\text{Yb}^{3+}$  ions at around 1000 nm ( $^2\text{F}_{5/2} \rightarrow ^2\text{F}_{7/2}$ ) as a way of measuring temperature. Figure 2(b) shows the temperature dependence of the intensity ratio  $\Delta = I_{\text{Nd}}/I_{\text{Yb}}$  where  $I_{\text{Nd}}$  and  $I_{\text{Yb}}$  are defined as the emitted intensities at 1350 and 1000 nm, respectively. The error bars are associated with the experimental uncertainty in the determination of the luminescence intensity ratio. A linear fit to the experimental data allowed us to estimate the relative thermal sensitivity of our NPs (defined as  $S_r = (1/\Delta)|\partial\Delta/\partial T|$ ), providing us  $S_r = 0.74 \pm 0.02\% \text{ } ^\circ\text{C}^{-1}$  at 20 °C.<sup>12,36</sup> This is a remarkable value when compared with the relative thermal sensitivities previously reported for other luminescent NPs operating in the II-BW.<sup>11,37–39</sup> As mentioned, a large concentration of  $\text{Nd}^{3+}$  ions in the shell is

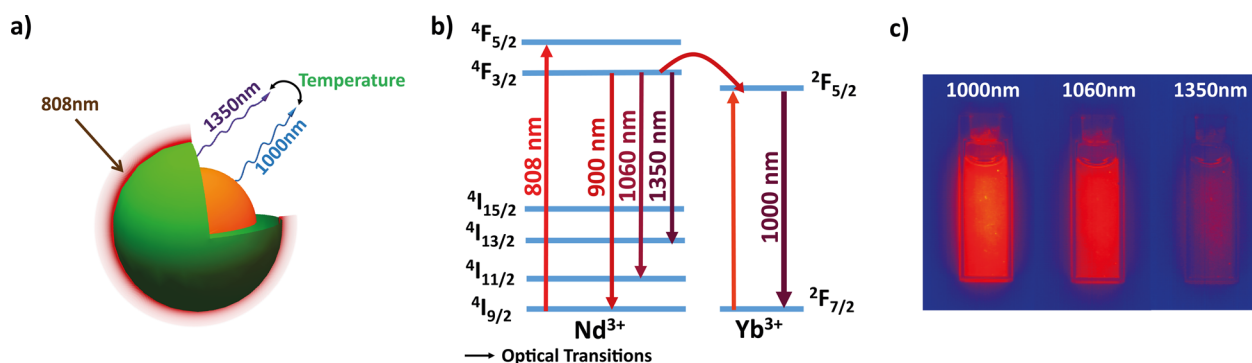


FIG. 1. (a) Schematic representation of the  $\text{Yb@Nd LaF}_3$  NPs used all along this work. (b) Simplified energy scheme of the  $\text{Nd}^{3+}$  and  $\text{Yb}^{3+}$  emitting centers representing excitation and radiative decays (full lines) and possible ion-ion energy transfer paths (curved lines). (c) Infrared fluorescence images of a cuvette containing the  $\text{Yb@Nd LaF}_3$  NPs at 1000, 1060, and 1350 nm. Specific filters were used to detect individual emission bands.

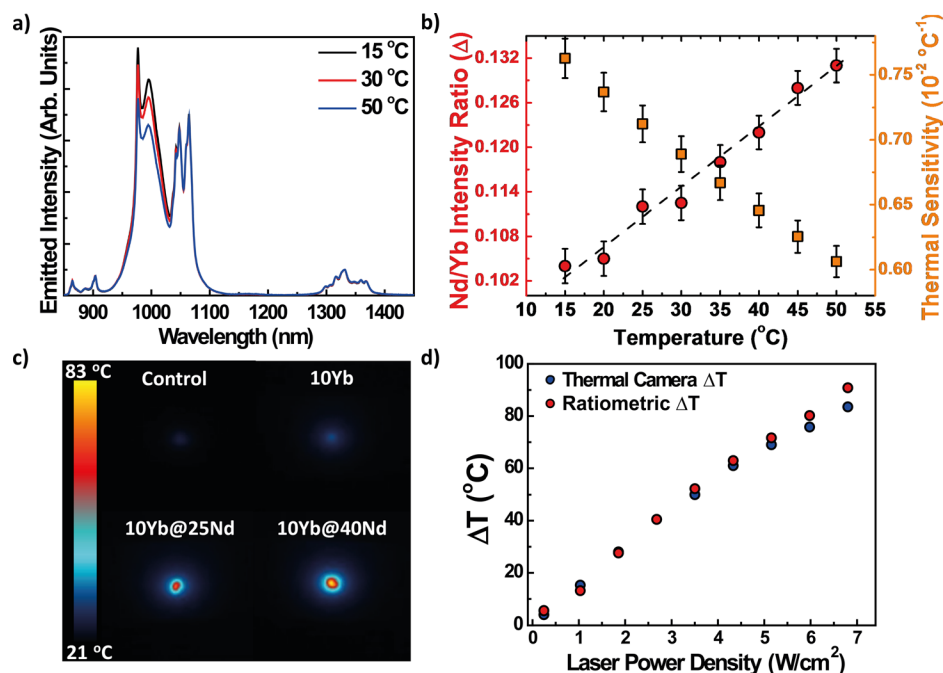


FIG. 2. (a) Emission spectra of Yb@Nd LaF<sub>3</sub> NPs obtained at 15, 30, and 50 °C under 808 nm excitation. (b) Calibration (red circles) and sensitivity (orange squares) curves of Yb@Nd LaF<sub>3</sub> NPs. Dots are experimental values, and the line represents the best fit to the experimental data using a linear function ( $r^2 > 0.913$ ). Power density used during calibration experiments was set to be 0.2 W/cm<sup>2</sup>. Error bars are associated with the experimental uncertainty in the determination of the luminescence intensity ratio. (c) Thermal images of powder containing NPs with different Nd<sup>3+</sup> concentration as obtained under 808 nm excitation and a laser power density of 3.4 W/cm<sup>2</sup>. Control corresponds to a microscope slide without Yb@Nd LaF<sub>3</sub> NPs. (d) Temperature variation of Yb@Nd LaF<sub>3</sub> NPs under different laser power densities obtained with infrared thermal camera and nanothermometer.

expected to provide heating capabilities to the nanostructure.<sup>33,36</sup> In order to corroborate this possibility and to demonstrate the dominant role played by Nd<sup>3+</sup> concentration in the light-to-heat efficiency of our NPs, a simple control experiment was conceived. Different core/shell NPs presenting the same Yb<sup>3+</sup> concentration into the core (10 mol. %) and different Nd<sup>3+</sup> concentrations into the shell (0, 25, and 40 mol. %) were exposed to an 808 nm laser radiation (with a power density of 3.4 W/cm<sup>2</sup>). The subsequent temperature variations were observed by infrared thermometry using a FLIR E40 thermal camera. In order to have a control reference, a measurement using only the holder was also done. The thermal images corresponding to the steady state temperatures of the NPs are presented in Figure 2(c). As it can be seen, the temperature of the NPs increases with the Nd<sup>3+</sup> concentration into the shell which can be well explained due to the fact that the larger the Nd<sup>3+</sup> concentration in the system is, the greater is the non-radiative delivered energy (the lower is the fluorescence quantum efficiency).<sup>40,41</sup> Thus, experimental data reveal the Nd<sup>3+</sup> ion content to be the main responsible source for the heating in accordance with previous studies centered on Nd<sup>3+</sup> single doped LaF<sub>3</sub> NPs.<sup>3</sup> The extent of agreement between the values provided by the thermal camera and the ratiometric nanothermometer while exposing the Yb@Nd LaF<sub>3</sub> NPs in powder (with concentrations of 10 mol. % for Yb<sup>3+</sup> ions into the core and 25 mol. % for Nd<sup>3+</sup> ions into the shell) to an 808 nm laser radiation was also estimated and the results are included in Figure 2(d). As it can be seen, differences between those measurements start to appear only for high values of laser power density (between 5.1 and 6.8 W/cm<sup>2</sup> it is possible to see differences ranging from 2.5 to 7 °C). Hereafter, the laser power densities used along the work were kept below 5 W/cm<sup>2</sup>.

Once the dual capability (heating + thermometry) of our Yb@Nd LaF<sub>3</sub> core/shell NPs was experimentally evidenced (see data included in Figure 2), their potential application in controlled photothermal processes was evaluated. Two

simple experiments, aiming to constitute clear proofs of concepts, were designed (see Figure 3(a)). In both experiments, we injected 0.2 ml of an aqueous solution of Yb@Nd LaF<sub>3</sub> NPs (10% in mass) into a chicken breast sample (injection depth estimated to be close to 2.0 mm). An 808 nm laser beam was focused into the injection by using a single long-working distance microscope objective (40×, N.A. 0.25). The Yb@Nd LaF<sub>3</sub> NPs would partially convert the 808 nm laser radiation into heat, producing a well localized temperature increase inside the tissue. The amount of this heating at the injection volume was estimated with the intensity ratio,  $\Delta$  (as defined above), from the infrared spectra generated at the injection volume. For this purpose, the luminescence generated by Yb@Nd LaF<sub>3</sub> NPs was collected by the same objective used for 808 nm laser focusing, and after passing several filters and confocal apertures, was spectrally analyzed by using a high resolution spectrometer. For the first experiment, an infrared thermal camera was coupled to the optical set-up in order to record the temperature of the tissue's surface and to demonstrate the differences between subcutaneous and surface temperatures (the latter being expected to be lower due to heat diffusion processes).<sup>3,32,33</sup> The steady state subcutaneous and surface temperatures were recorded for different 808 nm power densities and in both cases, a linear relationship was experimentally found (see Figure 3(b)). As expected, there are remarkable differences between subcutaneous and surface temperature, as demonstrated in previous studies dealing with *ex vivo* and *in vivo* PTTs based on heating nanoparticles.<sup>3,32,33</sup> Since the infrared thermal camera fails to provide a value for the subcutaneous temperature, the use of NThs is extremely necessary for the achievement of an accurate and remote control over PTTs.

Additionally, the same experimental set-up was used to demonstrate the capability of our core/shell NPs for real time subcutaneous measurements. For this experiment, the laser power density was fixed and the luminescence spectra generated by the core/shell NPs were taken in intervals of 400 ms



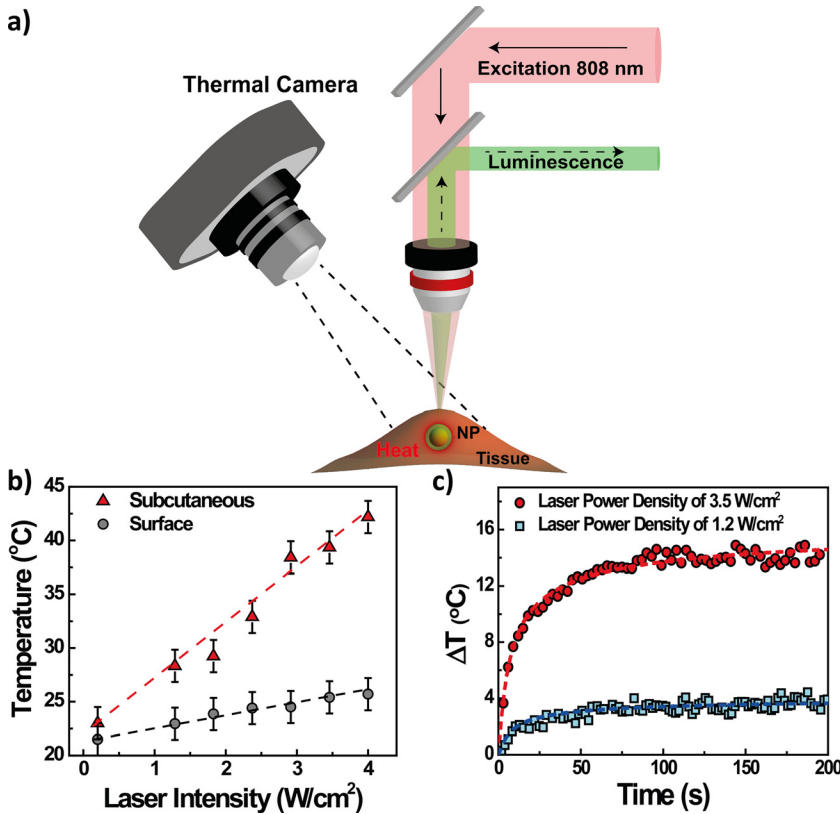


FIG. 3. (a) Schematic diagram of the *ex vivo* single beam experiment. The laser beam size is not drawn to scale. The spectral analysis of the injected core/shell nanoparticles provides the subcutaneous temperature whereas the surface temperature is recorded with an infrared thermo-camera. (b) Surface and subcutaneous temperatures as obtained for different 808 nm laser power densities. Dots are experimental data and dashed lines are linear fits. (c) Temperature stabilization of a tissue when exposed to an incident 808 nm laser beam at constant power density ( $1.2 \text{ W cm}^{-2}$  and  $3.5 \text{ W cm}^{-2}$  for blue squares and red circles, respectively).

for a time period of approximately 3 min (when thermal stabilization was achieved), starting when the laser was turned on. Figure 3(c) shows the time dependence of the subcutaneous temperature variation under two different excitation laser power densities, obtained computing the time evolution of the intensity ratio  $\Delta$  from the subcutaneous emission spectra. It should be noticed that the dynamic thermal reading demonstrated in Figure 3(c) was obtained using the same NPs that were inducing the subcutaneous heating. In our experimental conditions the laser spot size is orders of magnitude smaller than the heat dissipation length inside the tissue. Therefore, it is reasonable to consider the whole NP injection as a heating point source. According to literature, the temperature rise at a distance  $r$  from a small source of volume generating heat at a rate  $Q$  located in a homogeneous medium without perfusion is given by  $\Delta T(\vec{r}, t) = (Q/4\pi\alpha r) \text{erfc}(r/\sqrt{4\alpha t})$ , where  $\alpha$  is the thermal diffusivity of the medium.<sup>42,43</sup> Hence, the average temperature over a sphere of radius  $R$  around the heating point source is found to be

$$\Delta T_{\text{avg}}(t) = \Delta T_{\infty} \left( 1 + \left( \frac{t}{2\tau} - 1 \right) \text{erf} \left( \sqrt{\frac{\tau}{t}} \right) - \sqrt{\frac{t}{\pi\tau}} (e^{-\tau/t}) \right), \quad (1)$$

where  $\Delta T_{\infty}$  is the steady temperature increment and  $\tau$  is the relaxation time given by  $R^2/4\alpha$ . Fitting the experimental data, obtained with low ( $1.2 \text{ W cm}^{-2}$ ) and high laser power densities ( $3.5 \text{ W cm}^{-2}$ ), to Equation (1) provides the values of  $6.6 \pm 0.6$  and  $6.0 \pm 0.3 \text{ s}$  for  $\tau$ , respectively. Considering  $\alpha = 0.15 \text{ mm}^2 \text{ s}^{-1}$  as the thermal diffusivity of the tissue, we obtain  $R = 2.0 \pm 0.1$  for  $1.2 \text{ W cm}^{-2}$  and  $R = 1.9 \pm 0.1 \text{ mm}$  for  $3.5 \text{ W cm}^{-2}$ .<sup>44</sup> These values are, indeed, close to the

estimated depth of injection, i.e., the distance between the heating source (NP injection) and the heat sink (tissue–air interface). Thus,  $R$  defines the region where the set of NPs are simultaneously sensing temperature and meaningfully heating the medium. Data included in Figure 3 demonstrate that our core/shell NPs are capable of providing a steady state and time resolved thermal reading over a subcutaneous heating process activated by themselves, constituting, therefore, a proof for the potential of Yb@Nd LaF<sub>3</sub> NPs for thermally controlled subcutaneous PTTs.

In summary, we have demonstrated how core/shell nano-engineering allows for the development of all rare earth based nanostructures capable of simultaneous heating and thermal feedback. This possibility has been demonstrated in a Neodymium and Ytterbium doped core/shell LaF<sub>3</sub> nanoparticle. While the core of the nanoparticle was doped with Yb<sup>3+</sup> ions, the surrounded shell was heavily doped with Nd<sup>3+</sup> ions so that it behaves as a heating unit. It was evidenced that the ratio between the Yb<sup>3+</sup> and Nd<sup>3+</sup> infrared emissions in our core/shell structure provides a full optical method for remote thermal reading. It has been experimentally demonstrated how, when the core/shell structure was optically excited with a single 808 nm infrared beam, the heating and sensing capabilities of these multifunctional nanoparticles are simultaneously activated. The application of our rare earth doped core/shell LaF<sub>3</sub> nanoparticles for the achievement of fully controlled photothermal processes under single infrared beam excitation in tissue environments has been demonstrated. Thus, the results here reported open up an avenue toward the development of PTTs with enhanced efficiency and reduced risk based on the use of rare earth doped core/shell structures.

This work was supported by the Spanish Ministerio de Economía y Competitividad (MAT2013-47395-C4-1-R), by Brazilian Agencies: FINEP (Financiadora de Estudos e Projetos) through the Grant Nos. INFRAPESQ-11 and INFRAPESQ-12; CNPq (Conselho Nacional de Desenvolvimento Científico e Tecnológico) Grants INCT NANO(BIO)SIMES and Project Universal No. 483238/2013-9; CAPES (Coordenação de Aperfeiçoamento de Pessoal de Ensino Superior) by means of the Project PVE No. A077/2013. Erving C. Ximendes is supported by a Ph.D. scholarship from CNPq and currently by the PVE A077/2013 Project by means of a Ph.D. sandwich program developed at the Universidad Autónoma de Madrid, Spain. Prof. Dr. Daniel Jaque is the PVE (Pesquisador Visitante Especial) of the Project No. A077/2013. Dr. K. U. Kumar is a post-doctoral fellow of this Project. Dr. Uéslen Rocha is supported by a Post Doctoral Fellowship grant PDE/CAPES at the Universidad Autónoma de Madrid-Spain through the Project No. 2108-14-3.

- <sup>1</sup>A. M. Gobin, D. P. O'Neal, D. M. Watkins, N. J. Halas, R. A. Drezek, and J. L. West, *Lasers Surg. Med.* **37**, 123 (2005).
- <sup>2</sup>X. Huang, I. H. El-Sayed, W. Qian, and M. A. El-Sayed, *J. Am. Chem. Soc.* **128**, 2115 (2006).
- <sup>3</sup>E. Carrasco, B. del Rosal, F. Sanz-Rodríguez, Á. J. de la Fuente, P. H. Gonzalez, U. Rocha, K. U. Kumar, C. Jacinto, J. G. Solé, and D. Jaque, *Adv. Funct. Mater.* **25**, 615 (2015).
- <sup>4</sup>X. Huang and M. A. El-Sayed, *Alexandria J. Med.* **47**, 1 (2011).
- <sup>5</sup>L. Tong, Q. Wei, A. Wei, and J.-X. Cheng, *Photochem. Photobiol.* **85**, 21 (2009).
- <sup>6</sup>D. Jaque, L. Martinez Maestro, B. del Rosal, P. Haro-Gonzalez, A. Benayas, J. L. Plaza, E. Martin Rodriguez, and J. Garcia Sole, *Nanoscale* **6**, 9494 (2014).
- <sup>7</sup>M. Johannsen, U. Gneveckow, L. Eckelt, A. Feussner, N. WaldÖfner, R. Scholz, S. Deger, P. Wust, S. A. Loening, and A. Jordan, *Int. J. Hyperthermia* **21**, 637 (2005).
- <sup>8</sup>J. B. Marmor, D. Pounds, T. B. Postic, and G. M. Hahn, *Cancer* **43**, 188 (1979).
- <sup>9</sup>W. C. Dewey, *Int. J. Hyperthermia* **10**, 457 (1994).
- <sup>10</sup>B. Hildebrandt, P. Wust, O. Ahlers, A. Dieing, G. Sreenivasa, T. Kerner, R. Felix, and H. Riess, *Crit. Rev. Oncol./Hematol.* **43**, 33 (2002).
- <sup>11</sup>E. C. Ximendes, W. Q. Santos, U. Rocha, U. K. Kagola, F. Sanz-Rodríguez, N. Fernández, A. d. S. Gouveia-Neto, D. Bravo, A. M. Domingo, B. del Rosal, C. D. S. Brites, L. D. Carlos, D. Jaque, and C. Jacinto, *Nano Lett.* **16**, 1695 (2016).
- <sup>12</sup>C. D. S. Brites, P. P. Lima, N. J. O. Silva, A. Millan, V. S. Amaral, F. Palacio, and L. D. Carlos, *Nanoscale* **4**, 4799 (2012).
- <sup>13</sup>D. Jaque and F. Vetrone, *Nanoscale* **4**, 4301 (2012).
- <sup>14</sup>S. Huang, S. Liu, K. Wang, C. Yang, Y. Luo, Y. Zhang, B. Cao, Y. Kang, and M. Wang, *Nanoscale* **7**, 889 (2015).
- <sup>15</sup>A. M. Smith, M. C. Mancini, and S. Nie, *Nat. Nano* **4**, 710 (2009).
- <sup>16</sup>A. N. Bashkatov, E. A. Genina, V. I. Kochubey, and V. V. Tuchin, *J. Phys. D: Appl. Phys.* **38**, 2543 (2005).
- <sup>17</sup>E. Hemmer, N. Venkatachalam, H. Hyodo, A. Hattori, Y. Ebina, H. Kishimoto, and K. Soga, *Nanoscale* **5**, 11339 (2013).
- <sup>18</sup>E. Hemmer, A. Benayas, F. Legare, and F. Vetrone, *Nanoscale Horiz.* **1**, 168 (2016).
- <sup>19</sup>C.-H. Quek and K. W. Leong, *Nanomaterials* **2**, 92 (2012).
- <sup>20</sup>J. T. Robinson, G. Hong, Y. Liang, B. Zhang, O. K. Yaghi, and H. Dai, *J. Am. Chem. Soc.* **134**, 10664 (2012).
- <sup>21</sup>K. Welsher, S. P. Sherlock, and H. Dai, *Proc. Natl. Acad. Sci.* **108**, 8943 (2011).
- <sup>22</sup>G. Hong, J. T. Robinson, Y. Zhang, S. Diao, A. L. Antaris, Q. Wang, and H. Dai, *Angew. Chem., Int. Ed.* **51**, 9818 (2012).
- <sup>23</sup>E. Cassette, M. Helle, L. Bezdetnaya, F. Marchal, B. Dubertret, and T. Pons, *Adv. Drug Delivery Rev.* **65**, 719 (2013).
- <sup>24</sup>F. C. J. M. van Veggel, *Chem. Mater.* **26**, 111 (2014).
- <sup>25</sup>R. Gui, H. Jin, Z. Wang, and L. Tan, *Coord. Chem. Rev.* **296**, 91 (2015).
- <sup>26</sup>M. Nyk, R. Kumar, T. Y. Ohulchanskyy, E. J. Bergey, and P. N. Prasad, *Nano Lett.* **8**, 3834 (2008).
- <sup>27</sup>X. Li, R. Wang, F. Zhang, L. Zhou, D. Shen, C. Yao, and D. Zhao, *Sci. Rep.* **3**, 3536 (2013).
- <sup>28</sup>Y. Zhang, G. Hong, Y. Zhang, G. Chen, F. Li, H. Dai, and Q. Wang, *ACS Nano* **6**, 3695 (2012).
- <sup>29</sup>L. Marciniak, K. Prorok, L. Frances-Soriano, J. Perez-Prieto, and A. Bednarkiewicz, *Nanoscale* **8**, 5037 (2016).
- <sup>30</sup>M. G. Lupo, F. Della Sala, L. Carbone, M. Zavelani-Rossi, A. Fiore, L. Lüer, D. Polli, R. Cingolani, L. Manna, and G. Lanzani, *Nano Lett.* **8**, 4582 (2008).
- <sup>31</sup>Y.-F. Wang, G.-Y. Liu, L.-D. Sun, J.-W. Xiao, J.-C. Zhou, and C.-H. Yan, *ACS Nano* **7**, 7200 (2013).
- <sup>32</sup>U. Rocha, K. Upendra Kumar, C. Jacinto, J. Ramiro, A. J. Caamaño, J. García Solé, and D. Jaque, *Appl. Phys. Lett.* **104**, 053703 (2014).
- <sup>33</sup>E. C. Ximendes, U. Rocha, C. Jacinto, K. U. Kumar, D. Bravo, F. J. Lopez, E. M. Rodriguez, J. Garcia-Sole, and D. Jaque, *Nanoscale* **8**, 3057 (2016).
- <sup>34</sup>S. González-Pérez, I. R. Martín, F. Rivera-López, and F. Lahoz, *J. Non-Cryst. Solids* **353**, 1951 (2007).
- <sup>35</sup>D. F. de Sousa, F. Batalioto, M. J. V. Bell, S. L. Oliveira, and L. A. O. Nunes, *J. Appl. Phys.* **90**, 3308 (2001).
- <sup>36</sup>L. G. Van Uitert, *J. Electrochem. Soc.* **114**, 1048 (1967).
- <sup>37</sup>U. Rocha, C. Jacinto da Silva, W. Ferreira Silva, I. Guedes, A. Benayas, L. Martínez Maestro, M. Acosta Elias, E. Bovero, F. C. J. M. van Veggel, J. A. García Solé, and D. Jaque, *ACS Nano* **7**, 1188 (2013).
- <sup>38</sup>E. N. Cerón, D. H. Ortgies, B. del Rosal, F. Ren, A. Benayas, F. Vetrone, D. Ma, F. Sanz-Rodríguez, J. G. Solé, D. Jaque, and E. M. Rodríguez, *Adv. Mater.* **27**, 4781 (2015).
- <sup>39</sup>L. Marciniak, A. Bednarkiewicz, M. Stefanski, R. Tomala, D. Hreniak, and W. Strek, *Phys. Chem. Chem. Phys.* **17**, 24315 (2015).
- <sup>40</sup>V. Lupei, A. Lupei, S. Georgescu, T. Taira, Y. Sato, and A. Ikesue, *Phys. Rev. B* **64**, 092102 (2001).
- <sup>41</sup>N. Pavel, V. Lupei, J. Saikawa, T. Taira, and H. Kan, *Appl. Phys. B* **82**, 599 (2006).
- <sup>42</sup>W. L. Nyborg, *Phys. Med. Biol.* **33**, 785 (1988).
- <sup>43</sup>F. J. Reynoso, C.-D. Lee, S.-K. Cheong, and S. H. Cho, *Med. Phys.* **40**, 073301 (2013).
- <sup>44</sup>L. Huang and L.-S. Liu, *J. Food Eng.* **95**, 179 (2009).